Measurement-Based Multi-Link Massive MIMO Channel Characterization at Millimeter-Wave Bands

Lyu, Yejian; Mbugua, Allan Wainaina; Yuan, Zhiqiang; Fan, Wei

Published in:
17th European Conference on Antennas and Propagation, EuCAP 2023

DOI (link to publication from Publisher):
10.23919/EuCAP57121.2023.10133456

Publication date:
2023

Measurement-Based Multi-link Massive MIMO Channel Characterization at Millimeter-Wave Bands

Yejian Lyu[1], Allan Wainaina Mbugua[12], Zhiqiang Yuan[13], and Wei Fan[14]
[1]Antenna, Propagation, and Millimeter-wave Systems Section, Aalborg University, 9220 Aalborg, Denmark,
{yely, wfa}@es.aau.dk
[2]Huawei Technologies Duesseldorf GmbH, Munich Research Center, 80992 Munich, Germany, allan.mbugua@huawei.com
[3]Beijing University of Posts and Telecommunications, 100876 Beijing, China, yuanzhiqiang@bupt.edu.cn
[4]Center for Wireless Communication-Radio Technology (CWC-RT), Oulu, Oulu University, Finland.

***Abstract*—This paper presents a multi-user channel measurement campaign using a recently developed VNA-based multi-link channel sounder in an indoor hall scenario. The channel sounder architecture and comparison with the conventional multi-link channel sounder are firstly demonstrated, with a focus on the cost-effectiveness of the developed channel sounder. The two multi-user location combinations are considered in these channel measurements. The empirical channel data for the multi-user is then processed using the calibration procedure. By using the classical beamforming algorithm, the power-angle-delay-profiles (PADPs) are obtained from the calibrated channel response. The channel characteristics of the two links, i.e., PADP, delay and angular spread, are analyzed and compared.**

***Index Terms*—Multi-link, Channel measurements, mmWave, phase-compensation.**

I. Introduction

Massive multiple-input multiple-output (MIMO) has emerged as a critical technology for fifth-generation (5G) and future communication systems, allowing several users to share the same time-frequency resource [1], [2]. The massive MIMO performance is strongly dependent on the spatial distributions of the multiple users. Thus, proper knowledge of the realistic spatial channels for multiple users in the real-world deployment scenarios is crucial.

The huge potential of massive MIMO has led to the development of the multi-link channel sounders which have been used in channel measurement campaigns to explore the multi-user channel at sub-6 GHz bands [3], [4] and millimeter-wave (mmWave) bands [5], [6]. In the literature, state-of-the-art multi-link channel sounders are mainly based on two techniques: time-domain and frequency-domain. Channel sounders using time-domain techniques in combination with real antenna array (RAA) are typically utilized in dynamic massive MIMO channels. The main advantage of time-domain techniques is the high sampling rate and free operation of the transmitter (Tx) and receiver (Rx) [3], [4]. The tether-free operation of the Tx and Rx is nonetheless the main drawback of time-domain techniques due to the complexity of clock synchronization between the Tx and Rx. Furthermore, as the frequency and the amount of transceiver chains increase, the system cost increases significantly, and the calibration becomes more complicated.

As for channel sounders using frequency-domain techniques, the vector network analyzer (VNA)-based channel sounder is popular for investigating the MIMO channels in combination with the virtual antenna array (VAA) concept.However, two constraints limit the VNA use in MIMO channels in long-range scenarios, i.e., high signal loss in the radio frequency (RF) cables and the port resource limitation. The first limitation is that since the signal generator and analyzer are co-located in the VNA, we need to extend the antennas connected to the VNA via RF cables. The VNA-based channel sounders are typically employed in short-range measurement applications since the signal attenuation in RF cable reduces the dynamic range of the sounder, partically at mmWave frequencies. This limitations can be solved by radio-over-fiber (RoF) techniques since the signal attenuation in the optical fiber is significantly lower than that in the RF cable [7]. However, the application of RoF methods in phase-coherent measurements is constrained since the signal phase in the fiber is intrinsically sensitive to temperature change and mechanical stress of the fibers. The signal phase in the fiber can be stabilized by using the phase-compensation method [8], [9].

The VNA port resource also limits the amount of the transceiver chains for multi-user/multi-link channel investigations. This constraint can be overcome by using the optical delay line and combiner scheme. The orthogonality of the multi-link signals is maintained by the delay line. The combiner is utilized to combine all of the received signal and send the combined sigal to the one receiving port in the VNA [10], [11]. In [11], a cost-effective phase-compensated multi-link sounder at mmWave bands is proposed. The measurement range is increased by using the RoF scheme. By using a down-conversion scheme, the mmWave signal is down-converted to 10-60 MHz, where the phase change of the transmitted signal in the fiber is negligible. Furthermore, the port resource of the VNA can be saved by applying the delay line and combiner scheme at 10-60 MHz.

In this paper, the VNA-based multi-link phase-compensated channel sounder proposed in [11] is employed to measure multi-user channel measurements at 28 GHz. Note that only two links are considered in this study, however, this can be extended to up to 16 links. We measure two multi-user location

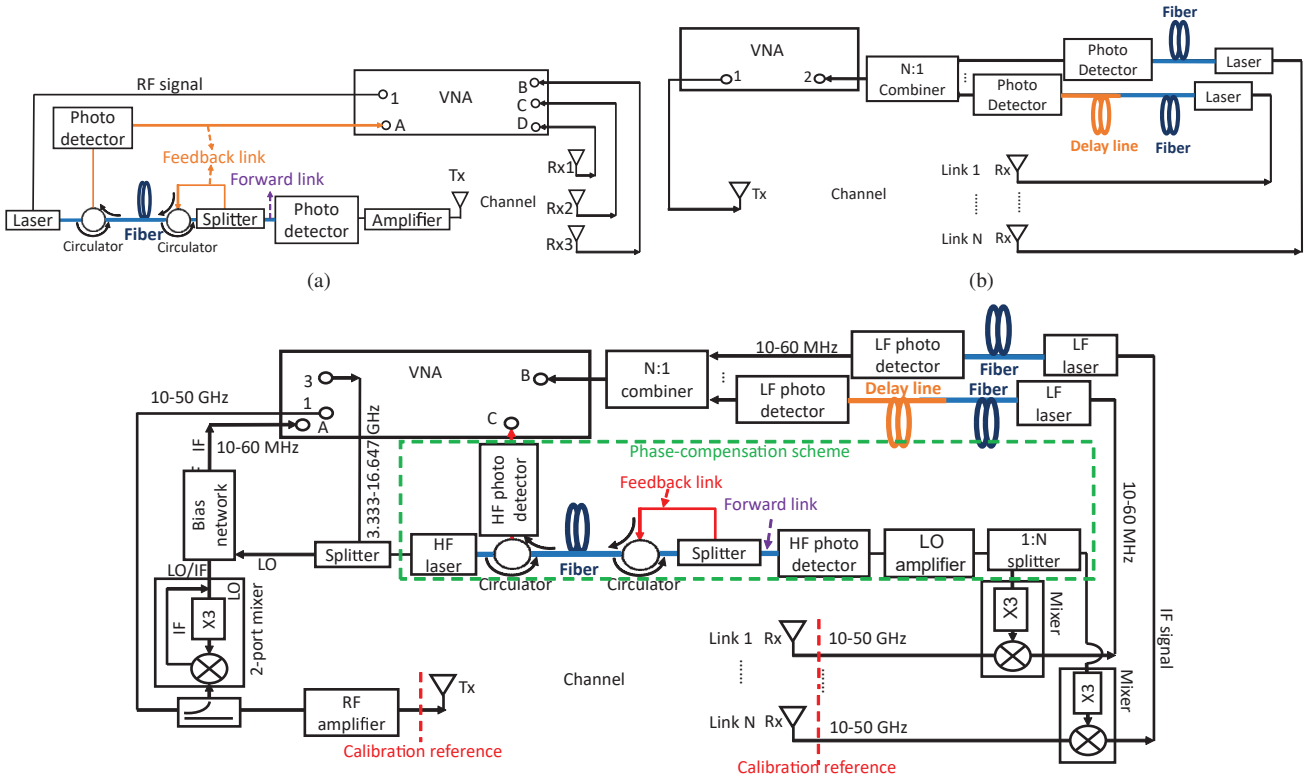

Fig. 1. Block diagrams of the channel sounder. (a) Conventional VNA-based multi-link channel sounder based on [8]. (b) Delay line and combiner scheme [10]. (c) Phase-compensated multi-link channel sounder [11].

combinations at the Rx side. The wideband spatial channel characteristics, i.e., power-angle-delay-profiles (PADPs), delay spread, and angular spread, for both links are also analyzed.

The remainder of this paper is structured as follows. The construction of the multi-link channel sounders at mmWave bands and the description of the measurement scenario are outlined in Section II. Section III analyses the detailed measurement results. Finally, concluding remarks are presented in Section IV.

II. Measurement Equipmemnt and Scenario

A. Channel Sounder Architecture

The conventional multi-link phase-compensated channel sounder is illustrated in Fig. 1 (a), which is the direct extension in [8] and is simple and straightforward to conduct the phase-coherent channel measurements. However, the receiving port source of commercial VNAs is limited. For example, Keysight N5227B VNA has up to five receiving ports, one port is used for receiving the reference signal on the Tx side and one port is occupied for the phase-compensation feedback link. Therefore, we only could achieve 3 multi-links by using the conventional sounder. In [10], a delay line and combiner scheme was proposed, which is a solution to port resource constraints. The scheme is depicted in Fig. 1 (b). However, at mmWave frequency bands, the phase performance of the optical delay line becomes unstable. Thus, it cannot be used for phase-coherent measurements. Due to the receiving port limitations, the phase-compensation schemes can only be applied to 3 links.

In [11], a cost-effective multi-link phase-compensated channel sounder is proposed and illustrated in Fig. 1 (c). Port 1 and Port 3 transmit the RF signal in the frequency range of 10-50 GHz, and the LO signal at 3.33-16.65 GHz, respectively. The RF signal is first split into two signals. One of the RF signals is transmitted through the channel by the Tx antenna and the other one is demodulated to intermedia frequency (IF) signal at 10-60 MHz and sent back to port A as a reference signal. The Rx received signal is demodulated to IF signal and sent through the low frequency (LF) RoF scheme (i.e., LF laser, fiber, and LF photo detector). Note that according to [12], the phase performance of the optical fiber cables at 10-60 MHz is stable. The IF signals is delayed by the delay line and all of those delayed signals are mixed by a combiner. Then the combined signal is sent to Port B. Thanks to the use of the down-conversion scheme, we only need to apply one phase-compensation scheme on the LO cable at the Rx side. Additionally, we only require one port to support multiple Rx links due to the delay line and combiner scheme.

B. Measurement Scenario

The multi-user channel measurements are conducted in an indoor scenario. The size of the room is $8.2 \times 4.8\,\mathrm{m}^2$. Fig. 2 depicts the measurement scenario. We set the Tx height and the

(a)

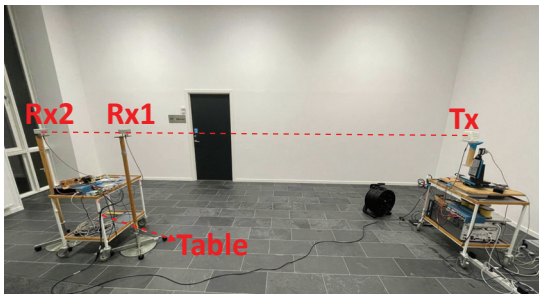

(b)

Fig. 2. Photo of the indoor scenario for two cases (a) Case 1 (b) Case 2.

Rx height to be the same as 1.45 m. A positioning stage is used at the Tx to implement a 23×30 virtual uniform rectangular array (URA) (i.e., 690 VAA elements) with an 0.4λ inter-element distance during the channel measurements. The VNA is configured to operate a frequency sweep from 28 to 30 GHz with a bandwidth of 2 GHz, a 20 kHz VNA IF bandwidth, and 1501 frequency points for each VAA element. The delay line can add a delay τ_{DL} to the optical signal transmission:

$$\tau_{DL} = \frac{L_{delay} \cdot B_{IF}}{c_{fiber} \cdot B_{RF}} \tag{1}$$

where L_{DL} denotes the optical delay line length. $c_{fiber} = 2.04 \times 10^8$ m/s represents the light speed in the fiber, BW_{RF} and BW_{IF} represent the bandwidth of the RF signal and IF signal, respectively. According to (1), the delay τ_{DL} caused by the optical delay line depends on the length L_{DL}, the bandwidth B_{RF}, and the bandwidth B_{IF}. Due to the use of the bias network, the bandwidth of the IF signal is limited in the frequency range of 10-60 MHz. Thus, the length of the delay line is set to be 1632 m. Note that a table is put between the two Rx links to support the RF components in the sounder. In the channel measurement campaign, we measure two Rx location combination cases: 1) As demonstrated in Fig. 2 (a), the Rxs are placed in the different LoS direction to the Tx. Link 1 (i.e., Tx-Rx 1) and Link 2 (i.e., Tx-Rx 2) have the same link distance of 4.17 m and the Rx 1-Rx 2 distance is 1 m. 2) Fig. 2 (b) depicts the scenario of Case 2. The Rxs are placed in the same LoS direction to the Tx. The Tx-Rx 1 distance is 4 m, and the Tx-Rx 2 distance is 5 m.

TABLE I
MEASUREMENT CONFIGURATION FOR THE TWO SCENARIOS.

Parameter	Value
Frequency (GHz)	28-30
VAA type	URA
Array size (x×y)	23×30
Inter-element distance (cm)	0.4
Number of points	1501
Transmitted power (dBm)	0
VNA IF bandwidth (kHz)	20
Antenna height (m)	1.45
Antenna type at Tx	Custom wideband biconical [13]
Antenna gain at Tx (dBi)	4.5
Number of Rx links	2
Antenna type at Rx	Biconical AINFO-SZ-2003000/P
Antenna gain at Rx (dBi)	5
Delay line length (m)	1632

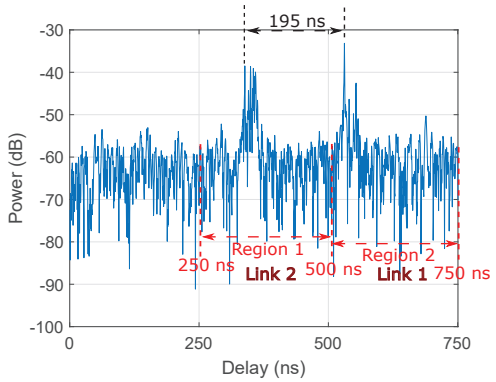

(a)

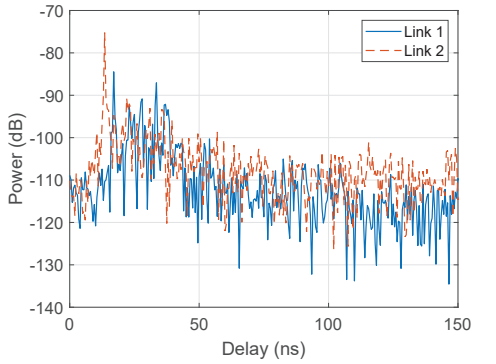

(b)

Fig. 3. Exemplary CIR results in Case 2. (a) CIR before calibration. (b) Calibrated CIR.

III. MEASUREMENT RESULTS

A. Data process

During the measurements, the received signals of each link are recorded in port B, and the frequency response is recorded as S_{BA}. Note that before the channel measurements, we remove the antennas and connect the Tx to each Rx to record the back-to-back system response for each link. In the post-processing, we first conduct the phase-compensation procedure using the recorded frequency response of the feed-back link. We then perform the inverse discrete Fourier

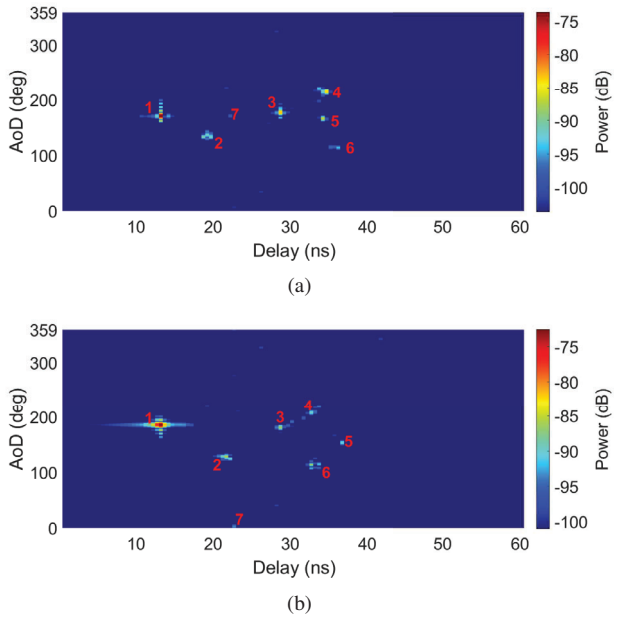

Fig. 4. PADP results using the classical beamforming algorithm in Case 1. (a) Link 1. (b) Link 2.

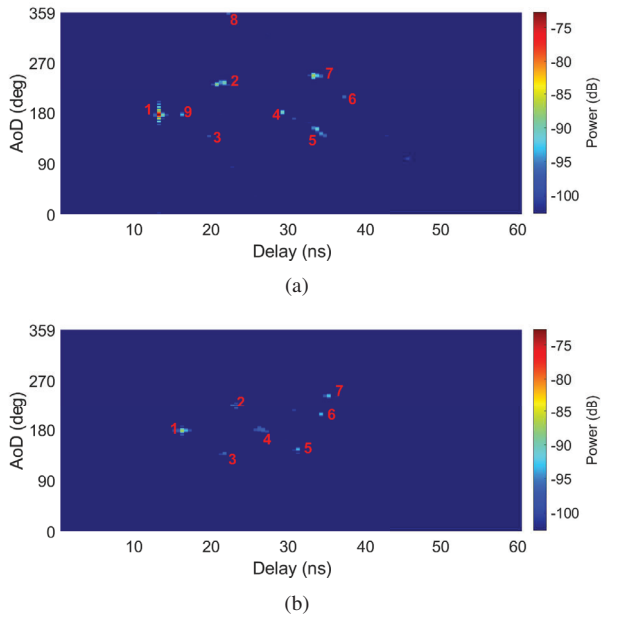

Fig. 5. PADP results using the classical beamforming algorithm in Case 2. (a) Link 1. (b) Link 2.

transform (IDFT) and use rectangular window functions with the specific delay range for each link in the delay domain to separate the response for Link 1 to Link N, i.e., $s_1(\tau), s_2(\tau - \Delta\tau), \ldots, s_n(\tau - (N-1)\Delta\tau)$. After separating the response for each link, we perform discrete Fourier transform (DFT) and apply the calibration procedure in the frequency domain. The detailed phase-compensation and calibration procedures can be referred to in [11]. The calibrated frequency responses are then processed using the classical beamforming algorithm [14] to obtain spatial-temporal channel characteristics. Fig. 3 illustrates the exemplary channel impulse response (CIR) before and after calibration. We can observe in the uncalibrated PDP that the paths of the two links are completely separated, as shown in Fig. 3 (a).

A 30-dB dynamic range is taken into account in relation to the line-of-sight (LoS) component's power in the measurement results. We also analyzed the delay spread and angular spread using the obtained delay and angle information of the identified paths. The detailed equations of the delay spread and angular spread can be referred to in [15].

B. Result and analysis

1) Case 1: The PADPs of both links are depicted in Fig. 4. Note that in this work, we only focus on the dominant paths. The delays of the LoS path in Link 1 and Link 2 are 13.5 ns and 14 ns, respectively. While the angle-of-departures (AoDs) of the LoS path in Link 1 and Link 2 are 171° and 186°, respectively. The relation of the identified multi-path components (MPCs) to the geometry of the indoor scenario can be referred in [11]. The delay spread and angular spread are calculated and illustrated in Table II. The delay spreads of the two links are shown to be close. However, the AoD spread of the Link 1 is observed to be 32.89° lower than that of Link 2 since the AoD range of the MPCs in Link 2 is $[2°, 208°]$, which is much wider than that in Link 1, i.e., $[113°, 215°]$.

2) Case 2: The PADPs of the two links are depicted in Fig. 5. We identify 9 and 7 dominant paths for the analysis of Link 1 and Link 2, respectively. The LoS path with an AoD of 177° and a delay of 13 ns is observed in Link 1, while the AoD and delay of the LoS path of Link 2 are seen to be 178° and 16.5 ns, respectively. The delay of the LoS path of the two links match the link distances between the Tx and the Rxs. The relationship between the identified MPCs and the geometry of the indoor scenario are depicted in Fig. 6. The LoS power of the both links are −72.69 dB and −86.70 dB. The Friis free-space path loss (FSPL) equation at 29 GHz is written as:

$$FSPL = 20 * \log_{10}\left(\frac{4\pi f d}{c}\right) = 20 * \log_{10} d + 61.69 \quad (2)$$

where f, c, and d denote the carrier frequency (i.e., 29 GHz), the speed of the light in vacuum, and the distance between the Tx and Rx, respectively. The theoretical value is calculated as −73.73 dB for Link 1 and −75.67 dB, respectively. The LoS power of Link 1 is close to the FSPL value. While the LoS power of Link 2 is 11.03 dB lower than the FSPL value due to the fact that the LoS of Link 2 is blocked by the Rx 1, which reduces the LoS power. Note that path 9 in Link 1 is observed to be the path from the ground reflection, and the ground reflection in Link 2 is seen to be blocked by the table. Besides, the identified path 1 and path 2-7 are observed to have a good similarity of the two links. The calculated delay spread and angular spread of the two links are illustrated in Table II. The delay spread and the AoD spread of Link 2 are observed to be 1.4 ns and 27.51° lower than those of Link 1, respectively,

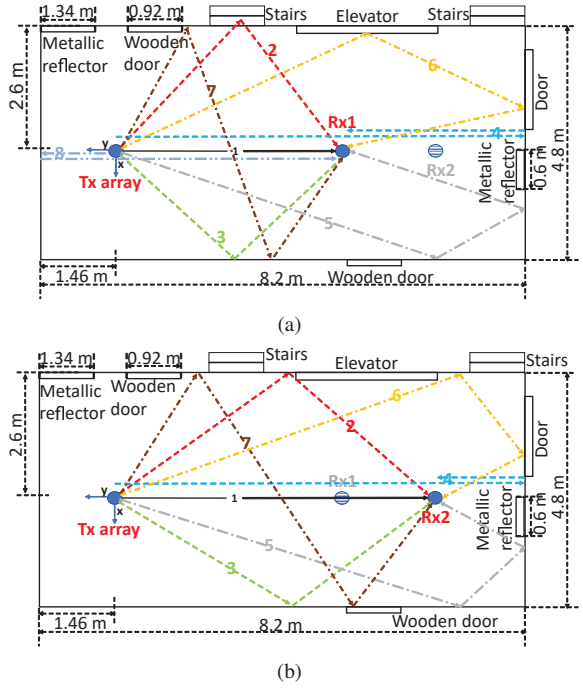

Fig. 6. Identified ray trajectory compared to room geometry in Case 2. (a) Rx 1. (b) Rx 2.

which is due to the blockage of the Rx 1 antenna and the fewer MPCs in Link 2.

TABLE II
DELAY SPREAD AND AOD SPREAD RESULTS OF THE TWO LINKS.

	Case 1		Case 2	
Parameter	Link 1	Link 2	Link 1	Link 2
Delay spread (ns)	8.04	7.32	7.86	6.46
AoD spread (°)	30.15	63.04	64.14	36.63

IV. CONCLUSION

In this paper, the multi-user channel characterization using the VNA-based multi-link channel sounder in an indoor hall scenario is presented. We first compare our channel sounder architecture with the conventional multi-link channel sounder and show the cost-effectiveness of the developed channel sounder. Then, we use the phase-compensation and calibration procedure in [11] to process the measured channel data. Then we use the classical beamforming algorithm to obtain the PADP. We observed attenuation of the LoS power in Link 2 due to the blockage of the Rx 1 antenna. The MPCs of both links in Case 2 are seen to have a good similarity. Besides, we also calculate and compare the delay spread and AoD spread of the two links. In future work, we plan to use precoding analysis for these two cases.

ACKNOWLEDGEMENT

The work was partially supported by the 21NRM03 MEWS project, which has received funding from the European Partnership on Metrology, co-financed from the European Unions Horizon Europe Research and Innovation Programme and by the Participating States.

REFERENCES

[1] E. G. Larsson, O. Edfors, F. Tufvesson, and T. L. Marzetta, "Massive MIMO for next generation wireless systems," *IEEE Communications Magazine*, vol. 52, no. 2, pp. 186–195, 2014.

[2] Z. Ma, B. Ai, R. He, Z. Zhong, and M. Yang, "A non-stationary geometry-based MIMO channel model for millimeter-wave UAV networks," *IEEE Journal on Selected Areas in Communications*, vol. 39, no. 10, pp. 2960–2974, 2021.

[3] l. O. Martnez, E. De Carvalho, and J. d. Nielsen, "Towards very large aperture massive MIMO: A measurement based study," in *2014 IEEE Globecom Workshops (GC Wkshps)*, 2014, pp. 281–286.

[4] A. Karstensen, J. . Nielsen, P. C. F. Eggers, E. De Carvalho, G. F. Pedersen, M. Alm, and G. Steinbck, "Multi-user spatial consistency analysis of outdoor massive-mimo measurements," *IEEE Transactions on Antennas and Propagation*, pp. 1–1, 2021.

[5] A. W. Mbugua, W. Fan, Y. Ji, and G. F. Pedersen, "Millimeter wave multi-user performance evaluation based on measured channels with virtual antenna array channel sounder," *IEEE Access*, vol. 6, pp. 12 318–12 326, 2018.

[6] J. Zhang, A. A. Glazunov, J. Yang, X. Chu, and J. Zhang, "An experimental study on indoor massive 3D-MIMO channel at 30-40 GHz band," in *2018 International Symposium on Antennas and Propagation (ISAP)*, 2018, pp. 1–2.

[7] F. Zhang, X. Ge, B. Gao, J. Wei, and S. Pan, "Phase stable radio distribution over optic cable by phase conjugation using an optical frequency comb," in *2015 International Topical Meeting on Microwave Photonics (MWP)*, 2015, pp. 1–4.

[8] A. W. Mbugua, W. Fan, K. Olesen, X. Cai, and G. F. Pedersen, "Phase-compensated optical fiber-based ultrawideband channel sounder," *IEEE Trans. Microw. Theory Techn.*, vol. 68, no. 2, pp. 636–647, 2020.

[9] Y. Lyu, A. W. Mbugua, K. Olesen, P. Kyosti, and W. Fan, "Design and validation of the phase-compensated long-range sub-THz VNA-based channel sounder," *IEEE Antennas and Wireless Propagation Letters*, pp. 1–1, 2021.

[10] S. Mahboob and S. B. Ram, "Vector channel-sounder using fiber delay lines to separate the channels," in *2017 IEEE International Symposium on Antennas and Propagation USNC/URSI National Radio Science Meeting*, 2017, pp. 1113–1114.

[11] Y. Lyu, A. W. Mbugua, Z. Yuan, K. Olesen, and W. Fan, "Design and validation of a multilink phase-compensated long-range ultrawideband VNA-based channel sounder," *IEEE Transactions on Microwave Theory and Techniques*, pp. 1–16, 2022.

[12] M. F. De Guzman, M. Hassan, and K. Haneda, "Uncertainty of millimeter-wave channel sounder due to integration of frequency converters," in *2021 17th International Symposium on Wireless Communication Systems (ISWCS)*, 2021, pp. 1–6.

[13] S. S. Zhekov, A. Tatomirescu, and G. F. Pedersen, "Antenna for ultra-wideband channel sounding," *IEEE Antennas and Wireless Propagation Letters*, vol. 16, pp. 692–695, 2017.

[14] H. Krim and M. Viberg, "Two decades of array signal processing research: the parametric approach," *IEEE Signal Processing Magazine*, vol. 13, no. 4, pp. 67–94, 1996.

[15] C. Ling, X. Yin, R. Mller, S. Hfner, D. Dupleich, C. Schneider, J. Luo, H. Yan, and R. Thom, "Double-directional dual-polarimetric cluster-based characterization of 7077 ghz indoor channels," *IEEE Transactions on Antennas and Propagation*, vol. 66, no. 2, pp. 857–870, 2018.